

Direct Synthesis and Design of a General Sequentially Coupled Wideband Bandpass Filter With N -Transmission Zeros

Zhiliang Li and Ke-Li Wu, *Fellow, IEEE*

Abstract—This paper presents a general sequentially coupled wideband bandpass filter and its direct synthesis and design theory. The filter can achieve the same number of controllable transmission zeros (TZs) as that of resonators above the passband. Each resonator consists of a pair of shunt connected capacitively loaded stub and a grounded inductive stub. Resonators are connected through a short section of transmission line with designated electric length. The short connecting lines allow the filter a wide spurious free stopband. For given specifications and prescribed TZs, the elementary lumped element circuit model can be directly synthesized. Three basic lumped element circuit building blocks are approximated by legitimate distributed element circuits with which the wideband distributed element circuit can be systematically obtained. To demonstrate the performance of the proposed filter configuration and the effectiveness of the developed theory, a fourth and an eighth order of filter prototypes were designed and measured, showing the promising potential for practical applications.

Index Terms—Bandpass filter, Chebyshev response, inline, microstrip, synthesis, transmission zeros (TZs), wideband filter.

I. INTRODUCTION

WITH the advances of wireless communication systems, people have witnessed the evolution of three generations over the past 15 years from analog to advanced digital modulations. The latest generation of the wireless system not only occupies more frequency bands, but also needs to accommodate the coexistence with the systems of earlier generations. Therefore, there is an inevitable trend to build a heterogeneous network with which wireless communication of different working bands are integrated to share some common infrastructure equipment, such as antennas and outdoor radio units, as much as possible.

To combine signals of multiple bands and to provide sufficient isolation between channels, a combiner using wideband channel filters with controllable transmission zeros (TZs) would be a convenient choice. To this end, the synthesis and

design techniques of a wideband filter with designated TZs become a popularly concerned research subject. Although the coupling matrix concept has been extensively used to design the narrowband filters with finite TZs [1], it is not suitable for the design of a wideband filter as it does not involve the frequency dispersion of both resonators and coupling elements. In [2] and [3], the coupling matrix is extended to wide bandwidth cases by taking into the frequency dependence of couplings, which finds yet few applications. Besides the coupling matrix approach, various wideband bandpass filters have been designed on the basis of commensurate TEM transmission lines [4]–[6], the cascaded low-pass/high-pass filters [7]–[9], multiple-mode resonators [10], ring resonators [11]–[13], and so on. To introduce TZs for a wideband filter, many ways are proposed [14]–[17]. In [14], TZs are generated to enhance the skirt selectivity of the conventional stub bandpass filter by introducing the I/O cross coupling. In [15] and [16], two transmission paths are exploited to achieve signal cancellation at TZ frequencies. In [17], a short-circuited multi-conductor transmission line (MTL) is shunted between two series MTLs to generate two TZs on both sides of the passband. Although an increasing number of wideband bandpass filters have been reported, most of them are based on the use of $\lambda/4$ or $\lambda/2$ lines, which usually suffers from the bulky layout size and closely located spurious resonance modes. Besides, only a few of them gives the systematic synthesis procedure to determine the circuit parameters. In the authors' opinion, a legitimate way to design a wideband filter is to develop an *ad-hoc* synthesize and design procedure of a valid circuit model for a specific filter configuration.

In [18], a type of compact bandpass filter that is capable of providing both wide bandwidth and multiple TZs above the passband is proposed. The filter adopts a semi-lumped resonator, which consists of a shunt connected stepped impedance stub and a grounded inductive stub, as shown in Fig. 1(a). When a step impedance stub resonates, the main trunk of the filter is short circuited and, hence, a TZ is introduced. Semi-lumped resonators are sequentially coupled by $\lambda/4$ transmission lines, which are simply treated as constant admittance inverters in the design methodology. Due to the narrowband nature of the inverters, the filter is recently redesigned by exploiting a two-step aggressive space-mapping optimization algorithm [19].

In this work, a more general filter configuration, as depicted in Fig. 1(b), is proposed. The main difference from the circuit

Manuscript received September 30, 2015; revised February 19, 2016; accepted March 17, 2016. Date of publication April 25, 2016; date of current version May 10, 2016. This work was supported in part by The Chinese University of Hong Kong under a postgraduate scholarship and in part by the Development and Reform Commission of Shenzhen Municipality under Grant Shen Fa Gai (2013) 1673. (Corresponding author: Ke-Li Wu.)

The authors are with the Department of Electronic Engineering, The Chinese University of Hong Kong, Shatin, Hong Kong, and also with the Shenzhen Engineering Laboratory of Wireless Locating Technology and System, Shenzhen Research Institute, The Chinese University of Hong Kong, Shatin, Hong Kong (e-mail: zlli@ee.cuhk.edu.hk; klwu@ee.cuhk.edu.hk).

Color versions of one or more of the figures in this paper are available online at <http://ieeexplore.ieee.org>.

Digital Object Identifier 10.1109/TMTT.2016.2549534

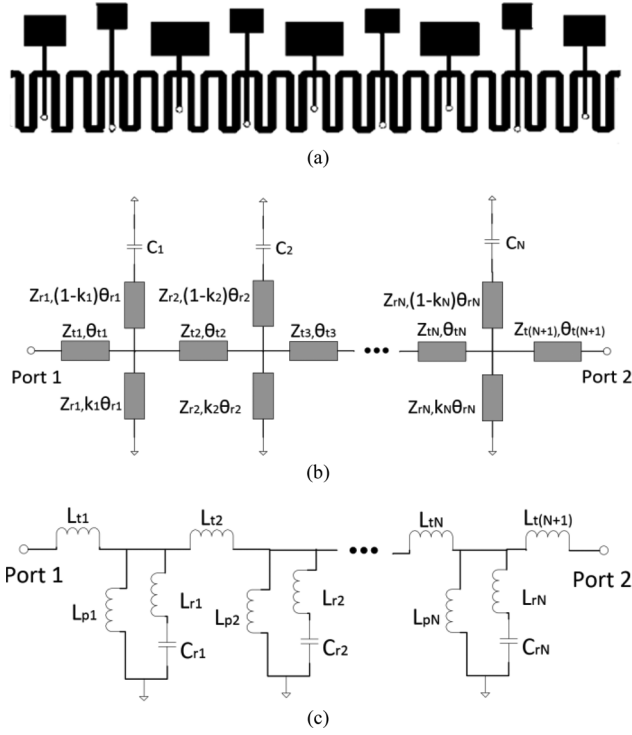


Fig. 1. (a) Topology of ninth-order filter designed in [18]. (b) Distributed circuit schematic of the wideband filter considered in this work. (c) Its lumped element circuit representation.

shown in Fig. 1(a) is that the connecting lines here can be as short as less than $\lambda/8$, and is designated by the designer. The new configuration benefits in the following ways. Firstly, the spurious resonance in the vicinity of twice center frequency f_0 introduced by the $\lambda/4$ connecting lines can be avoided; the concerning spurious resonance now mainly depends on resonators. Moreover, it helps shorten the main trunk of the filter and thus reduces the insertion loss. Importantly, the short connecting lines make the approximation of the lumped element circuit, as depicted in Fig. 1(c), by a distributed element circuit possible in a wide frequency range. Thanks to the approximation, the distributed element circuit can be directly synthesized by a two-step procedure. Firstly, the lumped element circuit is exactly synthesized for given specifications. The lumped element circuit is converted into a distributed element circuit based on an approximation of $ABCD$ matrices at critical frequencies for each coupling element and resonator.

This paper is organized as follows. Firstly, the approximation between a distributed element circuit and its lumped element circuit of each building block of the proposed filter structure is established in Section II. Section III elaborates the conversion from the directly synthesized lumped element circuit into the distributed element circuit. In Section IV, the properties and the synthesis procedure of the filtering function of the proposed filter are discussed, from which the lumped element circuit of the filter can be derived in Section V. As an important design parameter, the selection of rejection factor ε_0 will be discussed in detail in Section VI. Finally, two wideband filter design examples are given in Section VII from

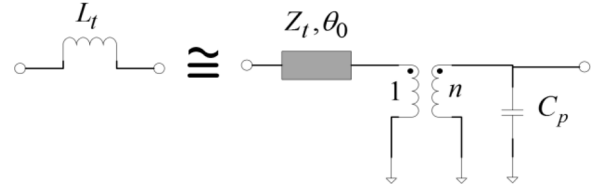


Fig. 2. Approximation of lumped element I/O coupling inductor.

design specifications to filter layout. Through the examples, the attractive features of the proposed filter are demonstrated.

II. APPROXIMATION AND TRANSFORMATIONS OF BASIC CIRCUIT ELEMENTS

In order to directly design the distributed element circuit that matches the synthesized lumped element circuit, one must find a set of appropriate basic distributed circuit elements that can replace the corresponding lumped circuit elements in a wideband sense. Concerning the approximated replacement, lumped elements in the synthesized circuit can be categorized into basic building blocks, i.e., the I/O coupling inductor, the inter-resonator coupling inductor, and the resonator.

A. Approximation of Lumped I/O Circuit by Distributed Circuit

As illustrated in Fig. 2, the lumped I/O circuit of a coupling inductor is approximated by a distributed circuit that consists of a short section of transmission line, an ideal transformer, and a shunt connected capacitor, all being cascaded. It will be shown later that the transformer and the shunt capacitor will be absorbed through circuit transformations. By equating the $ABCD$ matrices of the two circuits in Fig. 2 at the center frequency f_0 ,

$$\begin{aligned} \begin{bmatrix} 1 & j\omega_0 L_t \\ 0 & 1 \end{bmatrix} &= \begin{bmatrix} \cos \theta_0 & jZ_t \sin \theta_0 \\ jY_t \sin \theta_0 & \cos \theta_0 \end{bmatrix} \times \begin{bmatrix} \frac{1}{n} & 0 \\ 0 & n \end{bmatrix} \\ &\times \begin{bmatrix} 1 & 0 \\ j\omega_0 C_p & 1 \end{bmatrix} \\ &= \begin{bmatrix} \frac{\cos \theta_0}{n} - nZ_t \omega_0 C_p \sin \theta_0 & jnZ_t \sin \theta_0 \\ \frac{jY_t \sin \theta_0}{n} + jn\omega_0 C_p \cos \theta_0 & n \cos \theta_0 \end{bmatrix} \quad (1) \end{aligned}$$

the approximating circuit element can be obtained as

$$\theta_0 = \tan^{-1} \left(\frac{\omega_0 L_t}{Z_t} \right) \quad n = \sec \theta_0 \quad C_p = -\frac{\sin(2\theta_0)}{2\omega_0 Z_t} \quad (2)$$

where the characteristic impedance Z_t needs to be designated and can be exploited as a design freedom. Obviously, θ_0 decreases as Z_t increases. It can be observed, from Fig. 3, that the larger the Z_t is chosen, the better the approximation can be achieved in a wideband sense. The S -parameters are calculated at $f_0 = 1.7$ GHz and $L_t = 2.6$ nH by choosing Z_t as 50 and 120 Ω , respectively. It is seen from (1) and (2) that introducing the shunt connected C_p and the transformer

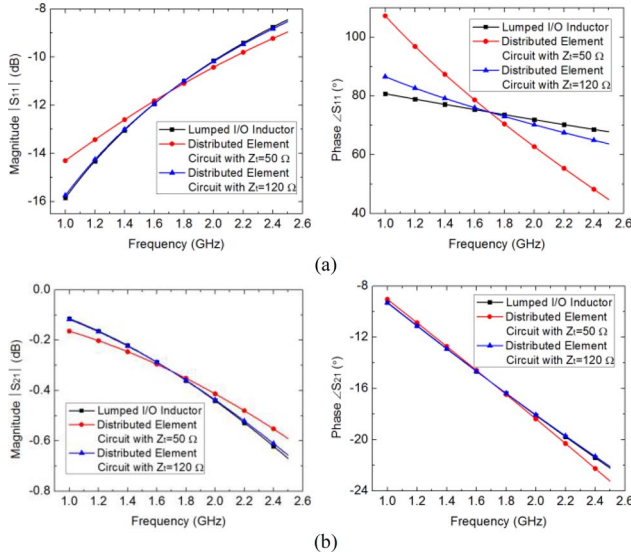


Fig. 3. Comparison between responses of lumped element I/O coupling inductor and distributed element circuits with $Z_t = 50 \Omega$ and 120Ω .

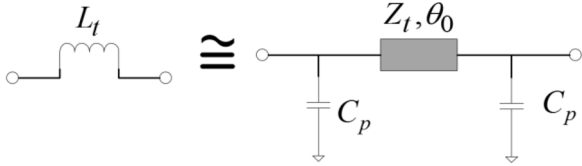


Fig. 4. Approximation of lumped element inter-resonator coupling inductor.

allow (1) being held to approximate an inductor using a short transmission line without introducing another negative shunt capacitor at the input port.

B. Approximation of Inter-Resonator Coupling Inductor

The inter-resonator coupling inductor can be approximated by a short transmission line with a shunt capacitor on each side, as depicted in Fig. 4. The shunt capacitance will be combined with that in a lumped circuit model of a short transmission line. Equating the $ABCD$ matrices of the two circuits at f_0 results in (3) as follows:

$$\begin{aligned} \begin{bmatrix} 1 & j\omega_0 L_t \\ 0 & 1 \end{bmatrix} &= \begin{bmatrix} 1 & 0 \\ j\omega_0 C_p & 1 \end{bmatrix} \times \begin{bmatrix} \cos \theta_0 & jZ_t \sin \theta_0 \\ jY_t \sin \theta_0 & \cos \theta_0 \end{bmatrix} \times \begin{bmatrix} 1 & 0 \\ j\omega_0 C_p & 1 \end{bmatrix} \\ &= \begin{bmatrix} \cos \theta_0 - \omega_0 C_p Z_t \sin \theta_0 & jZ_t \sin \theta_0 \\ (jY_t \sin \theta_0 + j2\omega_0 C_p \cos \theta_0 - j\omega_0^2 C_p^2 Z_t \sin \theta_0) & \cos \theta_0 - \omega_0 C_p Z_t \sin \theta_0 \end{bmatrix} \end{aligned} \quad (3)$$

which leads to the equivalence conditions

$$\theta_0 = \sin^{-1} \left(\frac{\omega_0 L_t}{Z_t} \right) \quad C_p = \frac{(\cos \theta_0 - 1)}{(\omega_0^2 L_t)} \quad (4)$$

where Z_t is chosen as a design freedom and is expected to be as large as possible for the sake of a good approximation in a wideband sense. By introducing C_p , (3) can be held for a short transmission line. For example, for $f_0 = 1.7$ GHz and

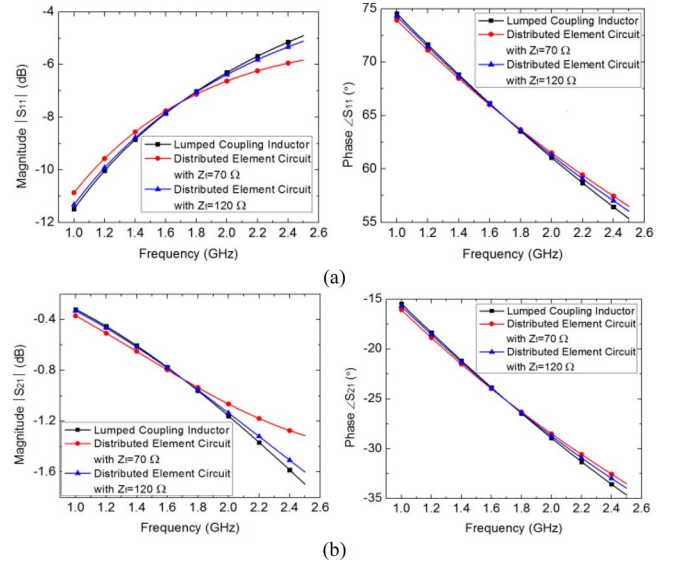


Fig. 5. Comparison between responses of lumped element coupling inductor and distributed element circuits with $Z_t = 70 \Omega$ and 120Ω .

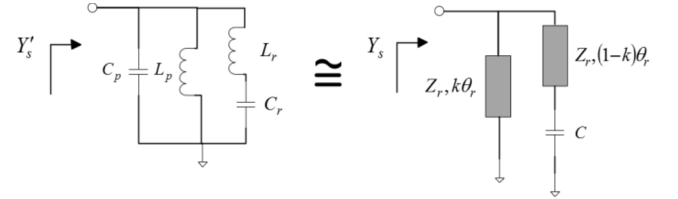


Fig. 6. Approximation of lumped element resonator by a distributed element resonator.

$L_t = 4.4$ nH, choosing Z_t as 70 and 120Ω , and calculating θ_0 and C_p by (4), the responses of the two circuit models are shown in Fig. 5. It can be observed that with a large Z_t the distributed circuit can well represent the ideal lumped inductor.

C. Approximation of Resonator Circuit

As illustrated in Fig. 6, the lumped resonant circuit is replaced by a distributed resonant circuit that consists of a capacitively loaded stub in parallel with a short-circuited stub. Note that the shunt capacitor C_p is generated from previous approximations. To approximate the lumped element resonant circuit by a distributed element circuit, one can equate their admittances at the lower band-edge frequency f_1 , the center frequency f_0 , and the upper band-edge frequency f_2 , i.e.,

$$\begin{aligned} Y'_s(f_i) &= Y_s(f_i) \\ &= -jY_r \cot \left(k \frac{f_i}{f_0} \theta_r \right) \\ &\quad + Y_r \frac{j\omega_i C + jY_r \tan \left(\frac{f_i}{f_0} (1-k) \theta_r \right)}{Y_r - \omega_i C \tan \left(\frac{f_i}{f_0} (1-k) \theta_r \right)}, \end{aligned} \quad i = 0, 1, \text{ and } 2 \quad (5)$$

through which parameters Y_r , C , and k for distributed circuits can be numerically solved. It is also noted the admittance

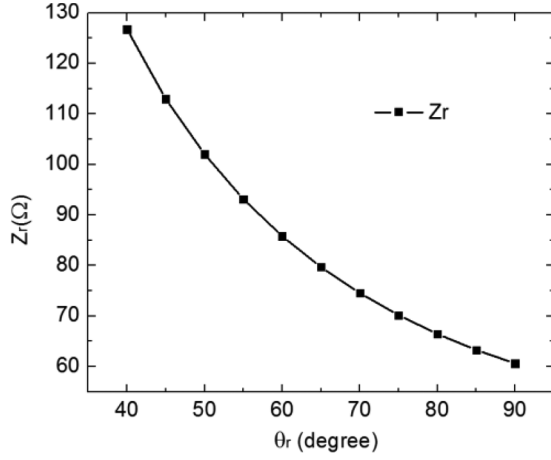


Fig. 7. Calculated characteristic impedance Z_r versus θ_r .

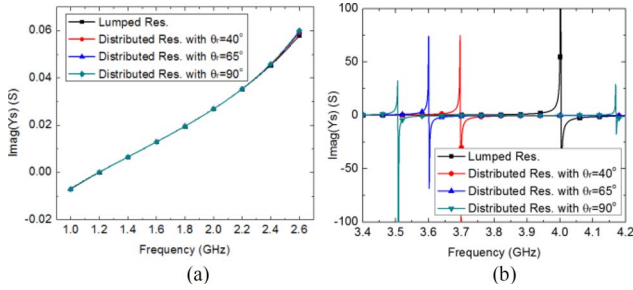


Fig. 8. Imaginary part of input admittances of lumped and distributed resonators with different θ_r : (a) in the passband and (b) in the upper stopband.

equivalence is only valid in the passband. In other words, the TZ will be relocated after the approximation.

In approximating the lumped circuit of a resonator, the electrical length θ_r is chosen as a design freedom. For example, for $f_1 = 1.4$ GHz, $f_0 = 1.7$ GHz, $f_2 = 2.1$ GHz, $C_p = -0.59$ pF, $L_p = 7.53$ nH, $C_r = 2.68$ pF, and $L_r = 0.59$ nH, the parameters of the distributed element circuit can be calculated by (5) with different θ_r . Fig. 7 shows the characteristic impedance Z_r versus θ_r . Observe that the characteristic impedance Z_r required becomes larger as θ_r decreases. The shortest θ_r is limited and mainly depends on the realizability of Z_r . For a typical microstrip realization, Z_r should not exceed 120Ω and, hence, θ_r has to be longer than 40° inferring from Fig. 7. To see how θ_r affects the approximation accuracy, the input admittances of lumped resonators and distributed resonators with $\theta_r = 40^\circ$, 65° , and 90° are compared in Fig. 8. It shows that the admittances are nearly the same in the passband $[f_1, f_2]$, but the admittance poles (TZs) are positioned differently. The TZs of the distributed resonator models are located closer to the passband as θ_r increases. This discrepancy can be accommodated by overshooting those TZs at higher frequencies.

It is also noted that there exists another TZ at 4.17 GHz when $\theta_r = 90^\circ$, as shown in Fig. 8(b). This is because the short-circuited stub acts as a $\lambda/2$ resonator at that frequency. For the cases of $\theta_r < 90^\circ$, the second TZ also exists, but is located even further away. It can be found that the spurious

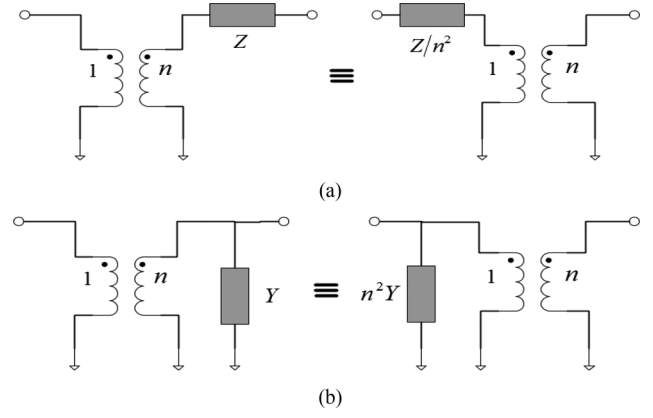


Fig. 9. Impedance or admittance scaling with a transformer. (a) Scaling of a serially connected impedance. (b) Scaling of a shunt connected admittance.

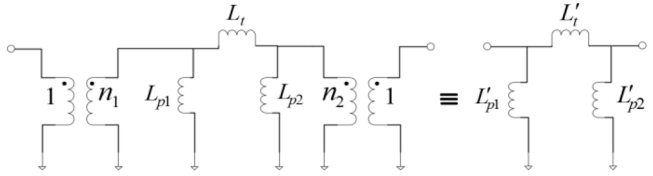


Fig. 10. Scaling of an inductive Π -circuit through two transformers.

resonance of the distributed resonator circuit approaches the passband as θ_r increases. Therefore, θ_r should be as short as possible to push the spurious resonance far away from the passband. Overall, there exists a tradeoff between the Z_r being moderate and the spurious resonance being far away from passband when choosing an appropriate θ_r .

D. Admittance Scaling and Transformer Transformations

Two basic circuit transformations will be used here to eliminate the two ideal transformers introduced for replacing the two I/O coupling inductors. One transformation is scaling of a serially connected impedance or shunt connected admittance, as illustrated in Fig. 9. The equivalence of this transformation is obvious and the equivalent circuit elements can be obtained in a straight manner. Another circuit transformation is scaling of an inductive Π -circuit through two transformers, as illustrated in Fig. 10, in which two ideal transformers on the two sides of a Π -network of inductors can be “absorbed” by the network. By equating their $ABCD$ matrices of the two circuits in Fig. 10 as

$$\begin{bmatrix} \frac{n_2}{n_1} \left(1 + \frac{L_t}{L_{p2}}\right) & s \frac{L_t}{n_1 n_2} \\ \frac{n_1 n_2 (L_{p1} + L_{p2} + L_t)}{s L_{p1} L_{p2}} & \frac{n_1}{n_2} \left(1 + \frac{L_t}{L_{p1}}\right) \end{bmatrix} = \begin{bmatrix} \left(1 + \frac{L'_t}{L'_{p2}}\right) & s L'_t \\ \frac{(L'_{p1} + L'_{p2} + L'_t)}{s L'_{p1} L'_{p2}} & \left(1 + \frac{L'_t}{L'_{p1}}\right) \end{bmatrix} \quad (6)$$

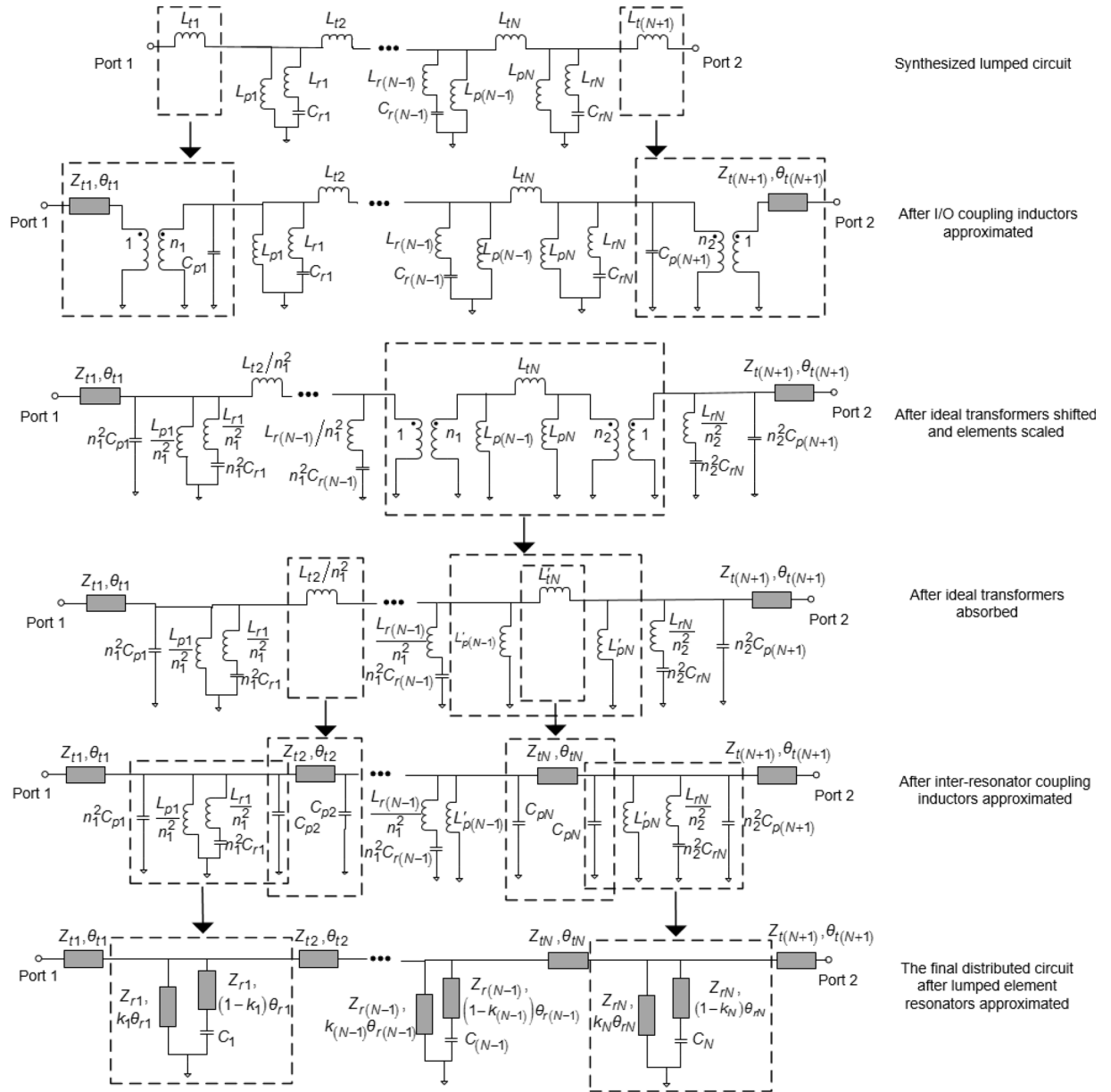


Fig. 11. Complete steps of the conversion process: approximating I/O coupling inductors, shifting ideal transformers with elements scaled, eliminating ideal transformers, approximating inter-resonator coupling inductors, and finally, lumped element resonators.

where $s = j\omega$, the updated inductances of the Π -network can be determined as

$$\begin{aligned} L'_t &= \frac{L_t}{n_1 n_2} \\ L'_{p1} &= \frac{L_t L_{p1}}{n_1 (L_{p1} (n_1 - n_2) + n_1 L_t)} \\ L'_{p2} &= \frac{L_t L_{p2}}{n_2 (L_{p2} (n_2 - n_1) + n_2 L_t)}. \end{aligned} \quad (7)$$

III. CONVERSION FROM LUMPED CIRCUIT INTO DISTRIBUTED CIRCUIT MODEL

Having introduced the required circuit approximations and transformations, the synthesized lumped element circuit shown in Fig. 1(c) can be converted into a distributed circuit shown

in Fig. 1(b) in order to directly design the filter layout. Fig. 11 illustrates the major steps in the conversion process: the process begins with the approximations of two I/O coupling inductors. The introduced transformers are then shifted to the sides of the shunt inductors of the $(N-1)$ th and N th resonator, respectively, using the admittance scaling. The two ideal transformers are absorbed by updating L_{tN} , $L_{p(N-1)}$, and L_{pN} using (7). With the second approximation, inter-resonator coupling inductors are replaced by short connecting lines. Finally, all lumped element resonators are approximated by distributed element resonators by adopting the third approximation. Having noted in the conversion, the shunt capacitor C_{pi} does not exist in neither the synthesized lumped element circuit, nor the final distributed element circuit, but actually acts as an intermediate element. In essence, it represents

the connecting-line-induced susceptance that perturbs adjacent resonators, and must be taken into account. Otherwise, the passband will have obvious frequency shift with deteriorated return loss after the conversion.

Due to the nature of the approximation, some deviations between the responses of the lumped element circuit and distributed element circuit will be inevitable. However, people may only be concerned with the response deviation in the passband and the discrepancy of the furthest TZs in filter design. Since the latter issue can be accommodated by over shooting the TZs, as discussed earlier, the key issue left is how to minimize the deviation in the passband. As noticed in previous illustrative examples, it is the approximation of coupling inductors instead of resonators that introduces the major deviation in the passband. A legitimate way to make the approximation accurate in a wide frequency range is either to choose a high characteristic impedance Z_l or to have a small coupling inductance. The first option is natural, but limited by the highest Z_l that can be realized. Fortunately, the second option is also available as there is a wide selection range of coupling inductances for a set of given passband, in-band return loss, and TZs, as will be discussed in Section VI.

IV. POLYNOMIAL FILTERING FUNCTION

By induction, it can be concluded that the overall $ABCD$ matrix of the lumped element circuit proposed in Fig. 1(c) can be written in the following form:

$$[ABCD] = \frac{1}{\sum_{i=0}^N p_{2i+1} s^{2i+1}} \times \begin{bmatrix} \sum_{i=0}^N a_{2i+1} s^{2i+1} & \sum_{i=0}^N b_{2i+2} s^{2i+2} \\ \sum_{i=0}^N c_{2i} s^{2i} & \sum_{i=0}^N d_{2i+1} s^{2i+1} \end{bmatrix} \quad (8)$$

where a_{2i+1} , b_{2i+2} , c_{2i} , d_{2i+1} , and p_{2i+1} are all real coefficients, and $p_{2N+1} = 1$, i.e., the denominator polynomial P , is monic. The corresponding scattering matrix $[S]$ can be obtained from the $ABCD$ matrix as

$$\begin{bmatrix} S_{11} & S_{21} \\ S_{12} & S_{22} \end{bmatrix} = \frac{1}{E} \begin{bmatrix} \frac{F}{\varepsilon} & \frac{P}{\varepsilon} \\ \frac{P}{\varepsilon} & F^* \end{bmatrix} = \frac{1}{\sum_{i=0}^{2N+2} e_i s^i} \times \begin{bmatrix} \sum_{i=0}^{2N+2} f_i s^i & \frac{\sum_{i=0}^N p_{2i+1} s^{2i+1}}{\varepsilon} \\ \frac{\sum_{i=0}^N p_{2i+1} s^{2i+1}}{\varepsilon} & \sum_{i=0}^{2N+2} (-1)^i f_i s^i \end{bmatrix} \quad (9)$$

where the coefficients e_i , f_i are real and $e_{2N+2} = 1$, $f_{2N+2} = 1$. Note that two constraints on polynomials need to be implied. The first one is that the roots of P must be all on the imaginary axis as the circuit produces N explicit finite TZs by shunt branches of series LC and a TZ at dc by shunt inductors. The second one is the existence of nonimaginary roots of F . Since E is real and strictly Hurwitz, its roots are either in a conjugate pair or on the negative real axis where the number of roots must be even because E is of even degree. Thus, the product of roots of E , i.e., e_0 , is positive.

As the main trunk of the filter is shorted to ground through the shunt inductors, the reflection coefficient $S_{11} = -1$ at dc, i.e.,

$$\left. \frac{F}{E} \right|_{s=j0} = \frac{f_0}{e_0} = -1. \quad (10)$$

From (10), f_0 , or the product of roots of F , is negative. Thus, nonimaginary roots do exist for F . Otherwise, f_0 must be positive, which contradicts with f_0 being negative.

According to the relation between the transmission coefficient and the filtering function,

$$|S_{21}|^2 = \frac{1}{1 + (\varepsilon F_N)^2} \quad (11)$$

where ε is the ripple factor, the required filtering function can be expressed as

$$F_N = \frac{F}{P} = \frac{s^{2N+2} + f_{2N+1} s^{2N+1} + \dots + f_1 s^1 + f_0}{s^{2N+1} + P_{2N-1} s^{2N-1} + \dots + P_3 s^3 + P_1 s}. \quad (12)$$

Under the imposed constraint that the roots of F are either on the imaginary axis of the complex s plane or symmetrically located about the imaginary axis, the odd-order term in F will vanish and, thus, the expression can be simplified to

$$F_N = \frac{F}{P} = \frac{s^{2N+2} + f_{2N} s^{2N} + \dots + f_2 s^2 + f_0}{s^{2N+1} + P_{2N-1} s^{2N-1} + \dots + P_3 s^3 + P_1 s}. \quad (13)$$

Due to the existence of nonimaginary roots, at most N roots of F can be located in the passband $[\omega_1, \omega_2]$ on the positive imaginary axis and naturally they have mirrors on the negative imaginary axis. The left two nonimaginary roots of F must then lie on the real axis because F is real and even.

To generate a generalized Chebyshev response (equiripple in the passband with specified TZs) for a specific filter circuit model, the filtering function should be appropriately developed. The conventional filtering function with a general Chebyshev characteristic used to synthesize a narrowband filter in the low-pass domain [1] does not generally fit a wideband filter. Instead, a bandpass filtering function needs to be specially developed for a wideband filter. In [2], a bandpass transversal equivalent circuit, which is able to create $N-1$ TZs with N resonators, is proposed. To introduce one more TZ, a Π -shaped network of inductors or capacitors can be added between the source and the load in the transversal circuit [20]. It can be verified that this modified circuit possesses the property

$$\frac{S_{11}|_{s=j0}}{S_{11}|_{s=j\infty}} = -1 \quad (14)$$

which demonstrates the existence of nonimaginary roots of F . To incorporate this property in the filtering function, a new term T_0 is introduced in the filtering function [20]. As a key feature, T_0 varies between $(0, 1]$ in the passband and equals to 1 at two band edges, which leads to the degree of F increased from $2N$ to $2N+2$, but possibly the number of imaginary roots of F remained to be $2N$. Specifically, the

filtering function can be expressed by

$$F_N(\omega) = \cosh \left(\cosh^{-1}(F_1(\omega)) + \sum_{k=2}^N \cosh^{-1}(f_k(\omega)) \right) \quad (15)$$

where

$$F_1(\omega) = \varepsilon_0 F_{1t}(\omega) = \varepsilon_0 (T_{0t}(\omega) f_{1t}(\omega) + G_t(\omega)) \quad (16)$$

$$T_0(\omega) = \frac{\omega^2 + \omega_1 \omega_2}{(\omega_1 + \omega_2)|\omega|} \quad (17)$$

$$f_k(\omega) = \frac{T_1(\omega) - \frac{1}{T_1(z_k)}}{1 - \frac{T_1(\omega)}{T_1(z_k)}} \quad (18)$$

$$T_1(\omega) = \frac{1}{\omega_2^2 - \omega_1^2} (2\omega^2 - (\omega_1^2 + \omega_2^2)) \quad (19)$$

$$G(\omega) = \frac{2\sqrt{(\omega_1^2 - z_1^2)(\omega_2^2 - z_1^2)(\omega^2 - \omega_1^2)(\omega^2 - \omega_2^2)}}{(\omega_1 + \omega_2)(\omega_2^2 - \omega_1^2)|\omega|(\omega^2 - z_1^2)} \quad (20)$$

$$\begin{cases} T_{0t}(\omega) = T_0(\omega) | \omega_1 = \omega_{1t}, \omega_2 = \omega_{2t} \\ f_{1t}(\omega) = f_1(\omega) | \omega_1 = \omega_{1t}, \omega_2 = \omega_{2t} \\ G_t(\omega) = G(\omega) | \omega_1 = \omega_{1t}, \omega_2 = \omega_{2t} \end{cases} \quad (21)$$

where $z_k (k = 1, \dots, N)$ are TZs, ω_1 and ω_2 are the lower and upper angular band edges, respectively. The rejection factor ε_0 is used to adjust the out-of-band rejection for a given bandwidth and TZs z_k . The intermediate frequencies ω_{1t} and ω_{2t} depend on ε_0 , and are calculated by the following criteria [20]:

$$F_1(\omega_1) = \varepsilon_0 F_{1t}(\omega_1) = -1 \quad F_1(\omega_2) = \varepsilon_0 F_{1t}(\omega_2) = 1. \quad (22)$$

From (15), the filtering function can be rephrased in a ratio of polynomials F and P , which can be obtained by a set of recursive processes [20]. It is found that the filtering function (13) is in the same form as that of (15), which satisfies the second circuit constraint and can be used to synthesis the proposed lumped element circuit shown in Fig. 1(c).

V. CIRCUIT MODEL EXTRACTION

Once the polynomials E , F , and P are obtained from the filtering function, the overall $ABCD$ matrix of the filter can be obtained. As a classical circuit synthesis approach, it is well described in [1] how to extract circuit elements sequentially from the $ABCD$ matrix for low-pass prototype filters. In [21], extracting procedures for some typical LC configurations have been explained by removal from an open-circuit or short-circuit impedance. To extract the circuit elements according to the circuit topology in Fig. 1(c), an $ABCD$ matrix is to be used here. Since each resonator is responsible for one finite TZ, how to arrange the TZs along the inline path from the input to the output should be determined beforehand. Obviously, the arrangement is not unique.

As shown in Fig. 12, with the TZs arranged, the whole extraction can be done in three phases, which are: 1) to extract a series inductor and a shunt branch of series LC ; 2) to extract a shunt inductor; and 3) to extract the remainder circuit

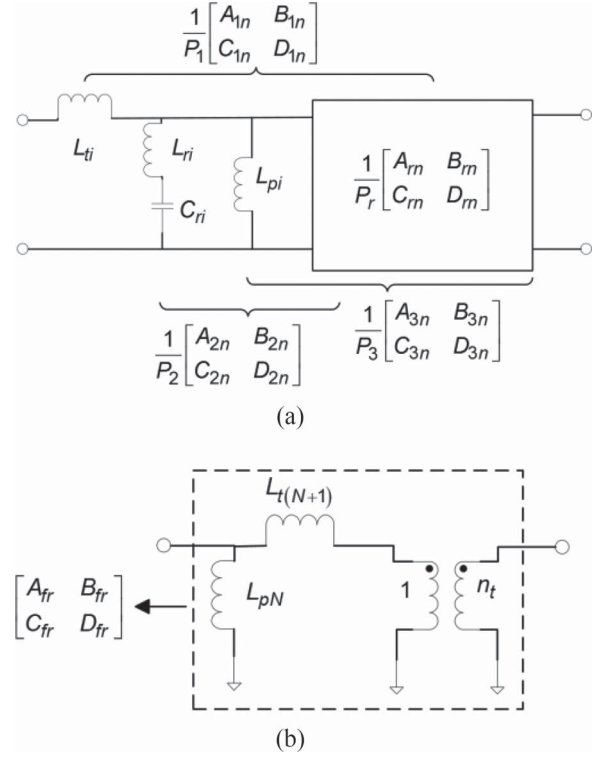


Fig. 12. Circuit element extraction scheme. (a) Extraction phase 1) and 2). (b) extraction phase 3).

that consists of L_{pN} , $L_{t(N+1)}$, and an ideal transformer with the transforming ratio $1:n_t$. Before proceeding to phase 3), it needs to repeat phases 1) and 2) N times and $N - 1$ times, respectively. The extracted circuit elements in phases 1) and 2) can be obtained through the following derivation:

$$\begin{aligned} & \frac{1}{P_1} \begin{bmatrix} A_{1n} & B_{1n} \\ C_{1n} & D_{1n} \end{bmatrix} \\ &= \frac{1}{P_2} \begin{bmatrix} A_{2n} + sL_{ti}C_{2n} & B_{2n} + sL_{ti}D_{2n} \\ C_{2n} & D_{2n} \end{bmatrix} \end{aligned} \quad (23)$$

$$\begin{aligned} & \frac{1}{P_2} \begin{bmatrix} A_{2n} & B_{2n} \\ C_{2n} & D_{2n} \end{bmatrix} \\ &= \frac{\begin{bmatrix} A_{3n}(s^2 - s_{zi}^2) & B_{3n}(s^2 - s_{zi}^2) \\ \frac{sA_{3n}}{L_{ri}} + C_{3n}(s^2 - s_{zi}^2) & \frac{sB_{3n}}{L_{ri}} + D_{3n}(s^2 - s_{zi}^2) \end{bmatrix}}{P_3(s^2 - s_{zi}^2)} \end{aligned} \quad (24)$$

$$\begin{aligned} & \frac{1}{P_3} \begin{bmatrix} A_{3n} & B_{3n} \\ C_{3n} & D_{3n} \end{bmatrix} \\ &= \frac{1}{P_r} \begin{bmatrix} A_{rn} & B_{rn} \\ A_{rn} \frac{1}{sL_{pi}} + C_{rn} & B_{rn} \frac{1}{sL_{pi}} + D_{rn} \end{bmatrix} \end{aligned} \quad (25)$$

where s_{zi} is the TZ assigned to the series L_{ri} and C_{ri} resonator circuit, the subscript n denotes the numerator polynomials, e.g., A_{1n} is the numerator polynomial of A_1 , etc. Since the series inductor does not contribute to any TZ, P_1 and P_2 share the same roots. Thus, without any scaling, $P_1 = P_2$. However, P_3 should not have the roots $\pm s_{zi}$ as the series L_{ri} and C_{ri}

have been extracted and, hence, is related to P_2 by

$$P_2 = P_3 (s^2 - s_{zi}^2). \quad (26)$$

From (23), $D_{1n} = D_{2n}$ and $B_{1n} = B_{2n} + sL_{ti}D_{2n}$. With $B_{2n}(s_{zi}) = 0$ from (24), the series inductance L_{ti} can be determined by

$$B_{2n}(s_{zi}) = B_{1n}(s_{zi}) - s_{zi}L_{ti}D_{1n}(s_{zi}) = 0 \text{ or } L_{ti} = \frac{B_{1n}(s_{zi})}{s_{zi}D_{1n}(s_{zi})}. \quad (27)$$

With L_{ti} known, $B_{2n} = B_{1n} - sL_{ti}D_{1n}$, and then B_{3n} can be obtained consequently by

$$B_{3n} = \frac{B_{2n}}{s^2 - s_{zi}^2}. \quad (28)$$

L_{ri} and C_{ri} can then be determined by

$$D_{2n}(s_{zi}) - B_{3n}(s_{zi}) \frac{s_{zi}}{L_{ri}} = 0 \text{ or } L_{ri} = \frac{s_{zi}B_{3n}(s_{zi})}{D_{2n}(s_{zi})} \quad (29)$$

and

$$C_{ri} = \frac{-1}{(s_{zi}^2 L_{ri})}. \quad (30)$$

In extraction phase 2), the shunt inductance L_{pi} should be designated as a design freedom. Since the shunt inductance is not totally extracted at node i , the remainder circuit still possesses a TZ at dc and, thus, $P_3 = P_r$. The remainder $ABCD$ matrix is determined from (25) after L_{pi} is excluded.

In extraction phase 3), the transforming ratio n_t is usually not equal to 1 unless L_{p1} through $L_{p(N-1)}$ are specially chosen in phase 2). The left elements in the remainder circuit can be determined by equating the remainder $ABCD$ matrix and the $ABCD$ matrix of the circuit in Fig. 12(b), i.e.,

$$\begin{bmatrix} A_{fr} & B_{fr} \\ C_{fr} & D_{fr} \end{bmatrix} = \begin{bmatrix} \frac{1}{n_t} & sn_t L_{t(N+1)} \\ \frac{1}{(sn_t L_{pN})} & n_t \left(1 + \frac{L_{t(N+1)}}{L_{pN}} \right) \end{bmatrix}. \quad (31)$$

Solving (31) leads to

$$n_t = \frac{1}{A_{fr}} \quad L_{t(N+1)} = \frac{A_{fr}B_{fr}}{s} \quad L_{pN} = \frac{A_{fr}}{sC_{fr}}. \quad (32)$$

Note that only B and D terms of the $ABCD$ matrix are used in extraction phase 1) and 2). Alternatively, it is also sufficient to determine the element values by using the A and C terms in these two phases.

As there is no ideal transformer in the target lumped element circuit, the transformations illustrated in Figs. 9 and 10 can be used here to eliminate the ideal transformer. To be specific, the extracted ideal transformer is shifted to the side of L_{pN} and, consequently, $L_{t(N+1)}$ has to be scaled. The transformer can then be absorbed into the Π network of L_{tN} , $L_{p(N-1)}$, and L_{pN} using (7). With $L_{p(N-1)}$ updated, the design freedom actually turns to be L_{p1} through $L_{p(N-2)}$, which leads to an infinite number of possible solutions even for the fixed arrangement of TZs. However, some of them are impractical because certain shunt inductances are so large that the approximations of resonator circuits will require stubs

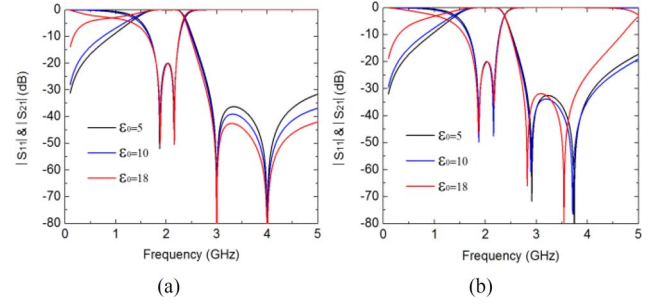


Fig. 13. Responses of: (a) lumped element circuit and (b) distributed element circuit for different rejection factor ε_0 .

of unrealizable high characteristic impedances. Even though extending the electrical length helps decrease the characteristic impedance requirement, it inevitably pushes the spurious resonance towards the passband. To ensure all the shunt inductors are realizable, the designation of L_{p1} through $L_{p(N-2)}$ should be appropriate through several iterations.

In particular, when both the TZs and the designated inductances are arranged symmetrically, the resultant lumped element circuit will be symmetrical. However, due to numerical errors, there would be some degree of asymmetry, especially for a high degree filter. To obtain a strictly symmetrical circuit, the extraction could be carried out alternately from the input port and the output port.

VI. SELECTION OF REJECTION FACTOR

As mentioned in Section IV, the rejection factor ε_0 should be designated to compute the filtering function. By choosing a large ε_0 , the upper stopband rejection could be enhanced as all TZs are located in the upper stopband. For illustration, a second-order filter, of which all circuit elements can be uniquely determined, is considered here. The center frequency is chosen to be 2 GHz with 400-MHz bandwidth (FBW = 20%). The two TZs are assigned at 3 and 4 GHz, respectively. The TZ embedded in F_1 is 3 GHz. The characteristic impedance of the connecting lines are set to be $Z_{t1} = Z_{t2} = Z_{t3} = 100 \Omega$, and the electrical length θ_r of resonators 1 and 2 are set to 60° at 2 GHz. The responses of the lumped element circuit and the distributed element circuit for different ε_0 are shown in Fig. 13. It can be observed that a larger ε_0 contributes to a larger rejection in the upper stopband of the lumped element circuit. However, the response of the distributed element circuit benefits little from the increased ε_0 . Actually, the location of TZs is the key factor that affects the stopband performance of the distributed circuit whereas ε_0 plays a secondary role. Therefore, ε_0 can be used to adjust circuit element values instead of out-of-band rejection. To ensure the circuit realizable, the value of ε_0 would be limited to a range. The lower bound of the range is determined by the I/O coupling inductances as they can be unrealizably negative for a small ε_0 . As ε_0 increases, the shunt inductances become larger and so do the characteristic impedances of stubs. Hence, the upper bound for ε_0 is governed by the realizable maximum characteristic impedance. In the achievable range of ε_0 , it prefers a moderate

TABLE I
CIRCUIT ELEMENT VALUES OF LUMPED ELEMENT CIRCUIT
FOR EXAMPLE 1

L_{li} (nH)	L_{pi} (nH)	L_{ri} (nH)	C_{ri} (pF)
$L_{l1}=2.591$	$L_{p1}=8.200$	$L_{r1}=0.6454$	$C_{r1}=2.453$
$L_{l2}=4.434$	$L_{p2}=8.200$	$L_{r2}=2.526$	$C_{r2}=1.605$
$L_{l3}=4.431$	$L_{p3}=8.249$	$L_{r3}=1.236$	$C_{r3}=2.278$
$L_{l4}=5.202$	$L_{p4}=8.355$	$L_{r4}=0.9578$	$C_{r4}=2.159$
$L_{l5}=2.381$			

TABLE II
CIRCUIT ELEMENT VALUES OF DISTRIBUTED
ELEMENT CIRCUIT FOR EXAMPLE 1

Z_{li} (Ω)	θ_{li} ($^\circ$) @ f_0	Z_{ri} (Ω)	θ_{ri} ($^\circ$) @ f_0	C_i (pF)	k_i
$Z_{li}=90$	$\theta_{l1}=17.09$	$Z_{r1}=76.13$	$\theta_{r1}=68$	$C_1=1.575$	$k_1=0.8585$
	$\theta_{l2}=28.73$	$Z_{r2}=91.10$		$C_2=0.9777$	$k_2=0.6252$
	$\theta_{l3}=28.71$	$Z_{r3}=78.58$		$C_3=1.511$	$k_3=0.7748$
	$\theta_{l4}=34.60$	$Z_{r4}=83.23$		$C_4=1.264$	$k_4=0.7977$
	$\theta_{l5}=15.78$				

or small ε_0 to well approximate coupling inductors over a wide band.

It is noteworthy that, not only ε_0 , but also filter order, fractional bandwidth, and return-loss requirement determine the realizability of design. For a fixed filter order, TZs, ε_0 , and electrical lengths of resonator stubs, larger shunt inductances, and hence, higher characteristic impedances of resonators are required to achieve a larger fractional bandwidth. Generally speaking, a larger fractional bandwidth or lower return-loss level is at the expense of poorer stopband rejection. Therefore, to realize a large fractional bandwidth and to enhance the stopband rejection, increasing the filter order is a convenient option.

VII. DESIGN EXAMPLES

The first design example is a fourth-order wideband band-pass filter with center frequency at 1.7 GHz, 40% fractional bandwidth, 20-dB in-band return loss, and four TZs arranged as 4, 2.5, 3, and 3.5 GHz, respectively, for the resonators counting from left to right.

The TZ embedded in F_1 is 4 GHz and the rejection factor for F_1 is chosen to be $\varepsilon_0 = 30$. It is worth mentioning that it does not matter to choose which finite TZ as z_1 in computing the filtering function. Actually, as long as the passband, z_k , and stopband rejection level are given, the filtering function is uniquely determined. The rational expression of the filtering function is obtained as (33), shown at the bottom of this page, where ω has been divided by $2\pi \times 10^9$. To make the shunt inductances nearly the same in all the resonators, the extraction has been done by several iterations with different trials of the inductance values. The finally extracted element values of the lumped element circuit and the distributed element circuit are listed in Tables I and II, respectively. The characteristic

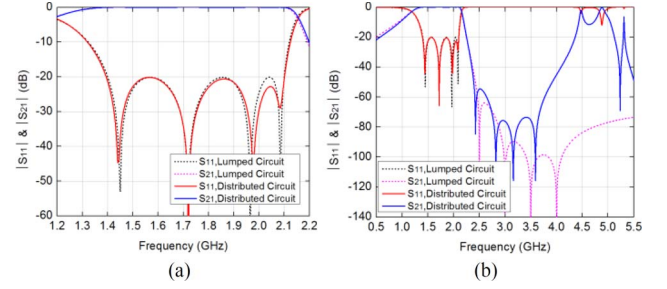


Fig. 14. Responses comparison: (a) in passband and (b) in a broad frequency range.

impedances of connecting lines are all set to be 90 Ω , whereas the electrical lengths of resonate lines all set to be 68° at the center frequency. As all the shunt inductances are nearly the same, the characteristic impedance of different resonate lines are similar to each other. Responses of the lumped element circuit and its converted distributed element circuit are compared in Fig. 14. The comparison shows that the responses agree very well in the passband, but the TZs of the distributed element circuit are lower than those achieved in the lumped element circuit.

To implement the design, a Rogers 5880 substrate with a dielectric constant of 2.2, loss tangent of 0.0009, thickness of 0.508 mm, and copper thickness of 0.017 mm is used. Having had the distributed circuit element values known, the line widths and lengths can be determined by available formulas characterizing microstrip line. The lumped capacitance to ground is realized by a radial stub in this design. The tapping point on each resonator line is estimated by the tapping ratio k_i ($i = 1, 2, 3$, and 4). The radial stub dimensions and tapping positions are then designed for each single resonator by comparing the responses of their electromagnetic (EM) models and their circuit models. After each resonator is designed, the initial filter layout can be generated by cascading all the designed resonators together with their connecting lines. Since the distributed circuit model can accurately describe the layout, the obtained initial response is sufficiently good. With slight optimization, the filter can be designed to meet the specifications. The layout and the photograph of the fabricated filter are shown in Fig. 15. The initial layout dimensions with further adjustments in parentheses by optimization is shown in Table III. The small dimension adjustments in the final design validate the effectiveness of the design approach. It is seen that the dimension adjustments are mainly on the lengths of connecting lines, which may be due to the parasitic couplings among adjacent resonators. The EM simulation (with loss) and the measured response are compared in Fig. 16. The first spurious resonance occurs at the frequency 2.5 times above the center frequency. The measured insertion loss is about 0.35 dB at lower band edge of 1.4 GHz, 0.41 dB at the

$$F_4(\omega) = \frac{0.9360\omega^{10} - 9.4608\omega^8 + 21.767\omega^6 + 59.596\omega^4 - 294.66\omega^2 + 300.33}{4.8298 \times 10^{-4}\omega^9 - 2.101 \times 10^{-2}\omega^7 + 3.2991 \times 10^{-1}\omega^5 - 2.2111\omega^3 + 5.3249\omega} \quad (33)$$

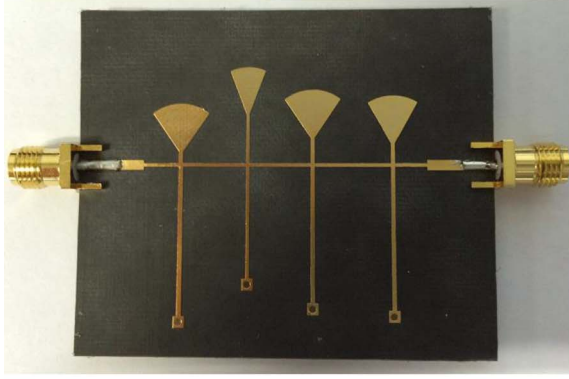
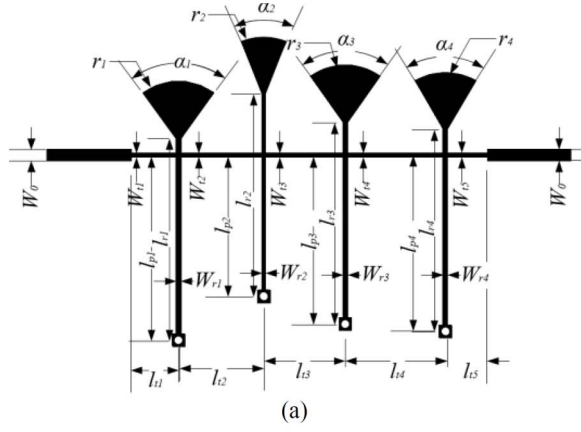


Fig. 15. (a) Layout and (b) fabricated fourth-order filter.

TABLE III
FILTER INITIAL LAYOUT DIMENSIONS AND ADJUSTMENTS IN PARENTHESES FOR EXAMPLE 1 (ALL DIMENSIONS ARE IN mm)

$W_0 = 1.40$	$l_{r1} = 24.40$	$l_{l1} = 6.44$ (-0.73)	$r_1 = 7.30$	$\alpha_1 = 72.3^\circ$
$W_{t1} = 0.45$	$l_{p1} = 21.98$	$l_{l2} = 10.84$ (-0.60)		$\alpha_2 = 43.9^\circ$
$W_{r1} = 0.62$	$l_{p2} = 16.80$	$l_{l3} = 10.82$ (-0.98)		$\alpha_3 = 72.1^\circ$
$W_{r2} = 0.45$	$l_{p3} = 20.13$	$l_{l4} = 12.98$ (-0.93)		$\alpha_4 = 56.7^\circ$
$W_{r3} = 0.58$	$l_{p4} = 20.78$	$l_{l5} = 5.94$ (-0.86)		$\alpha_5 = 72.1^\circ$
$W_{r4} = 0.55$				$\alpha_6 = 56.7^\circ$

center frequency of 1.7 GHz, and 1.03 dB at the upper band edge of 2.1 GHz.

The second design example is an eighth-order wideband bandpass filter with center frequency at 2 GHz, 50% fractional bandwidth, and 20-dB in-band return loss. Eight TZs are arranged symmetrically at 6, 5, 4, 3, 3, 4, 5, and 6 GHz, respectively, for the resonators counting from left to right.

The TZ embedded in F_1 is chosen to be 4 GHz and the rejection factor ε_0 is set to be 15. The rational expression of the filtering function is found as (34), shown at the bottom of

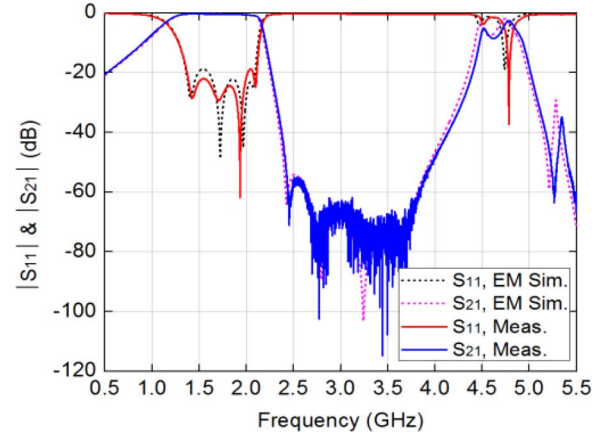


Fig. 16. Simulated versus measured response of the fourth-order filter.

TABLE IV
CIRCUIT ELEMENT VALUES OF LUMPED ELEMENT CIRCUIT FOR EXAMPLE 2

L_{li} (nH)	L_{pi} (nH)	L_{ri} (nH)	C_{ri} (pF)
$L_{l1}=2.450$	$L_{p1}=9.150$	$L_{r1}=0.3124$	$C_{r1}=2.252$
$L_{l2}=4.432$	$L_{p2}=3.850$	$L_{r2}=0.2898$	$C_{r2}=3.497$
$L_{l3}=3.541$	$L_{p3}=2.450$	$L_{r3}=0.4152$	$C_{r3}=3.813$
$L_{l4}=3.109$	$L_{p4}=7.567$	$L_{r4}=1.633$	$C_{r4}=1.724$
$L_{l5}=3.051$			

TABLE V
CIRCUIT ELEMENT VALUES OF DISTRIBUTED ELEMENT CIRCUIT FOR EXAMPLE 2

Z_{li} (Ω)	θ_{li} ($^\circ$) @ f_0	Z_{ri} (Ω)	θ_{ri} ($^\circ$) @ f_0	C_i (pF)	k_i
$Z_{l1}=100$	$\theta_{l1}=17.11$	$Z_{r1}=105.2$	$\theta_{r1}=60$	$C_1=1.733$	$k_1=0.9444$
$Z_{l2}=100$	$\theta_{l2}=30.58$	$Z_{r2}=46.87$	$\theta_{r2}=60$	$C_2=2.683$	$k_2=0.8894$
$Z_{l3}=80$	$\theta_{l3}=30.54$	$Z_{r3}=48.98$	$\theta_{r3}=40$	$C_3=3.229$	$k_3=0.8064$
$Z_{l4}=70$	$\theta_{l4}=30.65$	$Z_{r4}=97.67$	$\theta_{r4}=60$	$C_4=1.236$	$k_4=0.7203$
$Z_{l5}=70$	$\theta_{l5}=30.01$				

this page, where ω has been divided by $2\pi \times 10^9$. To ensure the extracted lumped element circuit symmetrical, the shunt inductance in each resonator from opposite ends share a common designated value. For the filter with a symmetric structure, the extraction is carried out alternately from the two opposite ends. In this example, the shunt inductances are arbitrarily designated. The extracted element values of the symmetrical lumped element circuit and the distributed element circuit are shown in Tables IV and V, respectively. The characteristic impedances Z_{l3} through Z_{l5} are chosen to be lower than 100 Ω to lengthen the connecting lines, which helps to reduce the parasitic coupling among adjacent resonators. Electrical length θ_{r3} is chosen to be 40° instead of 60° so that the characteristic

$F_8(\omega)$

$$= \frac{0.112\omega^{18} - 3.58\omega^{16} + 46.6\omega^{14} - 304\omega^{12} + 862\omega^{10} + 940\omega^8 - 1.52 \times 10^4\omega^6 + 4.82 \times 10^4\omega^4 - 6.96 \times 10^4\omega^2 + 3.95 \times 10^4}{7.40 \times 10^{-10}\omega^{17} - 1.27 \times 10^{-7}\omega^{15} + 9.27 \times 10^{-6}\omega^{13} - 3.73 \times 10^{-4}\omega^{11} + 9.05 \times 10^{-3}\omega^9 - 0.135\omega^7 + 1.22\omega^5 - 6.00\omega^3 + 12.4\omega} \quad (34)$$

- [4] R. J. Wenzel, "Exact design of TEM microwave networks using quarter-wave lines," *IEEE Trans. Microw. Theory Techn.*, vol. MTT-12, no. 1, pp. 94–111, Jan. 1964.
- [5] M. C. Horton and R. J. Wenzel, "General theory and design of optimum quarter-wave TEM filters," *IEEE Trans. Microw. Theory Techn.*, vol. MTT-13, no. 5, pp. 316–327, May 1965.
- [6] R. J. Wenzel, "Synthesis of combline and capacitively loaded interdigital bandpass filters of arbitrary bandwidth," *IEEE Trans. Microw. Theory Techn.*, vol. MTT-19, no. 8, pp. 678–686, Aug. 1971.
- [7] C.-L. Hsu, F.-C. Hsu, and J.-T. Kuo, "Microstrip bandpass filters for ultra-wideband (UWB) wireless communications," in *IEEE MTT-S Int. Microw. Symp. Dig.*, Jul. 2005, pp. 679–682.
- [8] R. Gomez-Garcia and J. I. Alonso, "Systematic method for the exact synthesis of ultra-wideband filtering responses using high-pass and low-pass sections," *IEEE Trans. Microw. Theory Techn.*, vol. 54, no. 10, pp. 3751–3764, Oct. 2006.
- [9] C. W. Tang and M. G. Chen, "A microstrip ultra-wideband bandpass filter with cascaded broadband bandpass and bandstop filters," *IEEE Trans. Microw. Theory Techn.*, vol. 55, no. 11, pp. 2412–2418, Nov. 2007.
- [10] L. Zhu, S. Sun, and W. Menzel, "Ultra-wideband (UWB) bandpass filters using multiple-mode resonator," *IEEE Microw. Wireless Compon. Lett.*, vol. 15, no. 11, pp. 796–798, Nov. 2005.
- [11] L. H. Hsieh and K. Chang, "Compact, low insertion-loss, sharp-rejection, and wideband microstrip bandpass filters," *IEEE Trans. Microw. Theory Techn.*, vol. 51, no. 4, pp. 1241–1246, Apr. 2003.
- [12] H. Ishida and K. Araki, "Design and analysis of UWB bandpass filter with ring filter," in *IEEE MTT-S Int. Microw. Symp. Dig.*, Jun. 2004, vol. 3, pp. 1307–1310.
- [13] S. Sun and L. Zhu, "Wideband microstrip ring resonator bandpass filters under multiple resonances," *IEEE Trans. Microw. Theory Techn.*, vol. 55, no. 10, pp. 2176–2182, Oct. 2007.
- [14] H. Shaman and J.-S. Hong, "Input and output cross-coupled wideband bandpass filter," *IEEE Trans. Microw. Theory Techn.*, vol. 55, no. 12, pp. 2562–2568, Dec. 2007.
- [15] J.-Y. Li, C.-H. Chi, and C.-Y. Chang, "Synthesis and design of generalized Chebyshev wideband hybrid ring based bandpass filters with a controllable transmission zero pair," *IEEE Trans. Microw. Theory Techn.*, vol. 58, no. 12, pp. 3720–3731, Dec. 2010.
- [16] W. J. Feng, W. Q. Che, Y. M. Chang, S. Y. Shi, and Q. Xue, "High selectivity fifth-order wideband bandpass filters with multiple transmission zeros based on transversal signal-interaction concepts," *IEEE Trans. Microw. Theory Techn.*, vol. 61, no. 1, pp. 89–97, Jan. 2013.
- [17] J. J. Sánchez-Martínez, E. Márquez-Segura, and S. Lucyszyn, "Synthesis and design of high-selectivity wideband quasi-elliptic bandpass filters using multiconductor transmission lines," *IEEE Trans. Microw. Theory Techn.*, vol. 63, no. 1, pp. 198–208, Jan. 2015.
- [18] J. Bonache, I. Gil, J. García-García, and F. Martín, "Compact microstrip band-pass filters based on semi-lumped resonators," *IET Microw. Antennas Propag.*, vol. 1, pp. 932–936, Aug. 2007.
- [19] M. Sans, J. Selga, A. Rodríguez, J. Bonache, V. E. Boria, and F. Martín, "Design of planar wideband bandpass filters from specifications using a two-step aggressive space mapping (ASM) optimization algorithm," *IEEE Trans. Microw. Theory Techn.*, vol. 62, no. 12, pp. 3341–3350, Dec. 2014.
- [20] R. Zhang and L. Zhu, "Synthesis of dual-wideband bandpass filters with source-load coupling circuit," *IEEE Trans. Microw. Theory Techn.*, vol. 62, no. 3, pp. 441–449, Mar. 2014.
- [21] R. Saal and E. Ulbrich, "On the design of filters by synthesis," *IRE Trans. Circuit Theory*, vol. CT-5, no. 4, pp. 284–327, Dec. 1958.



Zhiliang Li received the B.Eng. degree from the University of Electronic Science and Technology of China, Chengdu, China, in 2013, and is currently working toward the Ph.D. degree at The Chinese University of Hong Kong, Shatin, NT, Hong Kong.

His current research interests include passive RF and microwave circuits and filters.



Ke-Li Wu (M'90–SM'96–F'11) received the B.S. and M.Eng. degrees from the Nanjing University of Science and Technology, Nanjing, China, in 1982 and 1985, respectively, and the Ph.D. degree from Laval University, Quebec, QC, Canada, in 1989.

From 1989 to 1993, he was with the Communications Research Laboratory, McMaster University, as a Research Engineer and a Group Manager. In March 1993, he joined the Corporate Research and Development Division, COM DEV International, where he was a Principal Member of Technical Staff. Since October 1999, he has been with The Chinese University of Hong Kong, Hong Kong, where he is a Professor and the Director of the Radiofrequency Radiation Research Laboratory (R3L). His current research interests include partial element equivalent circuit (PEEC) and physics-based model-order reduction for electromagnetic (EM) modeling of high-speed circuits, RF and microwave passive circuits and systems, synthesis theory and computer-aided tuning of microwave filters, antennas for wireless terminals, low-temperature co-fired ceramic (LTCC)-based multichip modules (MCMs), and RF identification (RFID) technologies.

Prof. Wu is a Member of the IEEE MTT-8 Subcommittee (Filters and Passive Components) and also serves as a Technical Program Committee (TPC) Member for many prestigious international conferences including the IEEE Microwave Theory and Techniques Society (IEEE MTT-S) International Microwave Symposium (IMS). He was an Associate Editor for the IEEE TRANSACTIONS ON MICROWAVE THEORY AND TECHNIQUES from 2006 to 2009. He was the recipient of the 1998 COM DEV Achievement Award and the Asia-Pacific Microwave Conference Prize in 2008 and 2012, respectively.